EUROPEAN COMMISSION

HORIZON 2020 PROGRAMME - TOPIC H2020-LC-BAT-2019
Strongly improved, highly performant and safe all solid-state batteries for electric vehicles.

GRANT AGREEMENT No. 875189

SAFELiMOVE – Deliverable Report

<< D9.2 – Report on the process and upscale modelling >>

Deliverable No.	SAFELiMOVE D9.2	
Related WP	WP9	
Deliverable Title	Report on the process and upscale modelling	
Deliverable Date	08/12/2023	
Deliverable Type	REPORT	
Dissemination level	PUBLIC (PU)	
Written By	Arpit Mishra (ABEE)	2023-12-06
Checked by	Arpit Mishra (ABEE)	2023-12-19
Reviewed by (if applicable)	Mark Junker (RWTH), Elixabete Ayerbe (CID)	2023-12-20
Approved by	Maria Martinez (CICe)	2023-12-21
Status	Final	2023-12-21

Disclaimer/ Acknowledgment

This project has received funding from the European Union's Horizon 2020 research and innovation programme under grant agreement No 875189. The information and views set out in this publication does not necessarily reflect the official opinion of the European Commission. Neither the European Union institutions and bodies nor any person acting on their behalf, may be held responsible for the use which may be made of the information contained therein.

Publishable summary

In this detailed report, we investigate the complexities involved in scaling up battery sizes from small coin cells to larger 1 Ah and 10 Ah cells. The study focuses on the impact of processing technologies and design changes on battery performance during this transition. One of the key findings is that upscaling introduces new characteristics, such as variations in electrolyte conductivity and electrode porosity, which significantly influence discharge rates and overall efficiency. Our sensitivity analysis highlighted that, while electrolyte conductivity remains a critical factor in coin cells, in larger pouch cells, electrode porosity also plays a vital role. This dual significance poses unique challenges and opportunities in the design and optimization of larger batteries. The report concludes that despite these challenges, a careful and informed approach to parameter optimization can yield notable improvements in the performance of upscaled batteries. These insights are crucial for guiding the enhancement of battery design and manufacturing processes, especially in the context of transitioning from coin to pouch cells.

Executive summary

The document focuses on the upscale model developed to address the issues of upscaling from coin cells to pouch cells. The model was planned to be developed for a 10Ah cell earlier, but since the larger format cell was only 3.35, the model has adapted accordingly. A local sensitivity analysis is done on key changing parameters to understand the designing of the cells at a larger scale.

Contents

Figures

Tables

1 Introduction

In the relentless pursuit of advancing energy storage technologies, solid-state batteries have emerged as promising alternatives to conventional lithium-ion batteries, offering enhanced safety, higher energy density, and longer cycle life [1]. The transition from coin cell to pouch cell configurations represents a critical phase in the development and commercialization of solid-state batteries. This metamorphosis involves intricate processes and upscale modeling strategies aimed at optimizing performance, ensuring scalability, and addressing the unique challenges associated with the transition [2].
Coin cells, commonly employed in the early stages of solid-state battery research, provide a controlled environment for fundamental studies but need to improve in mirroring real-world applications. Pouch cells, on the other hand, offer a more practical and scalable design, making them a pivotal step in the journey from laboratory-scale innovations to market-ready solutions. The shift from coin cell to pouch cell demands a comprehensive understanding of the intricate processes involved, from material synthesis and electrode fabrication to cell assembly and testing.
This introduction delves into the complexities of the process and upscale modeling for solid-state batteries, exploring the critical considerations, advancements, and challenges associated with the transformation from coin cell prototypes to pouch cell configurations.

The report focuses on the work carried out in task 9.2. This report is divided into two more sections, followed by the conclusion of our findings. There is a section on model setup where we describe the general setup of the model with the governing equations. Further, the results are presented on the local sensitivity analysis performed in the key changing parameters such as electrode thickness, porosity, electrolyte conductivity and diffusivity; further, the results are used to infer the impact on dendrites formation and external pressure.

2 Modeling Framework

Introduction

In the deliverable 9.1, a p2d model was proposed for the coin cell to understand the sensitivity of different parameters. To carry forward this approach to upscale the model from coin cell to pouch cell, a similar approach is used for the pouch cell model, i. e., the continuum approach developed by Doyle and coworkers [3].

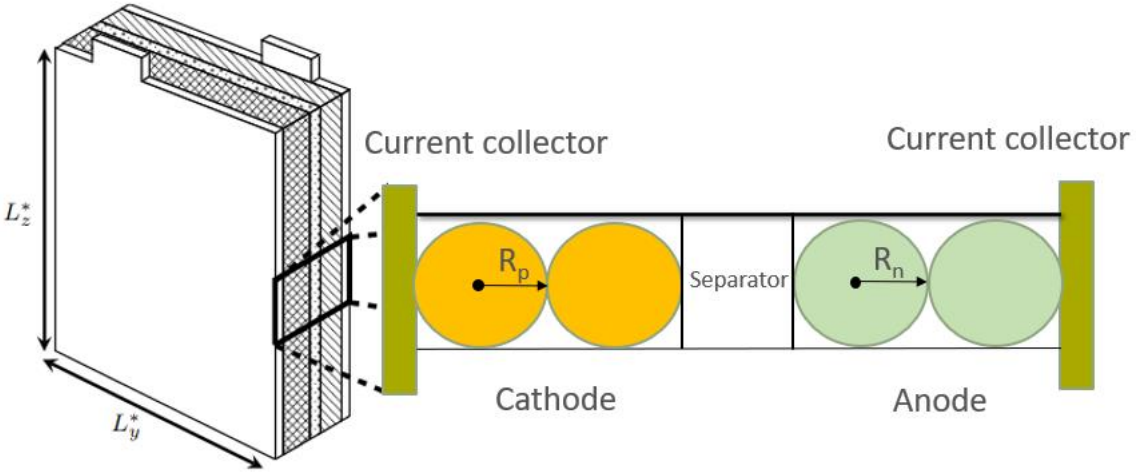

Figure 1 Schematic figure of P2D model for a pouch cell.

Model setup

The model represents the behavior of a lithium-ion pouch cell with the following layers: the negative and positive current collectors and in between them a negative electrode, a porous separator, a polymer electrolyte, and a positive electrode (see Figure 1) [4]. The electrodes are composed of porous particles, in which the active material is the core component that hosts lithium, all stuck together with a binder and conductive additives. This binder enhances the adhesion and cohesion of the electrodes while the conductive facilities the mobility of the electrons from the particles to the current collectors.

Using DFN approach [5, 6], a full 3D model of a lithium-ion pouch cell is developed as shown in Figure 1. Our model is detailed and includes the negative and positive current collectors, in addition to the usual parts of the DFN model: the negative electrode, the separator, and the positive electrode. The cell dimension for the pouch cell is taken from WP6. We treat these current collectors like paths for electricity to flow through easily.
In our model, we assume that the electric current comes out evenly from the positive tab, and the voltage at the negative tab stays steady at 0 V, which we use as our reference point. We determine the battery's voltage by looking at the average potential across the positive tab. Thermal effects are also considered by solving the thermal equation [7, 8].

Here we provide a detailed representation of a lithium metal anode, nickel manganese cobalt oxide (NMC)-based cathode, and a polymer electrolyte within the cathode as well as between the cathode and lithium domain. It accounts for the electrochemical reactions, material properties, and transport phenomena within the cell components. Below, the governing equations and assumptions for each component are presented.

2.1.1 Anode Modeling (Lithium Metal)

Electrochemical Kinetics: the lithium stripping and plating phenomena are represented by the Butler-Volmer equation:

$$i_{anode} = i_{o,anode}\left[\exp\left(\frac{\alpha_a F}{RT}\eta_{anode}\right) - \exp\left(-\frac{\alpha_c F}{RT}\eta_{anode}\right)\right] \quad (1)$$

where i_{anode} is the current density, $i_{o,anode}$ is the exchange current density, α_a and α_c are the anodic and cathodic charge transfer coefficients, F is Faraday's constant, R is the gas constant, T is the temperature, and η_{anode} is the anode overpotential.

Solid-State Diffusion: Lithium diffusion in the anode is governed by Fick's second law:

$$\frac{\partial c_{Li,anode}}{\partial t} = D_{Li,anode}\frac{\partial^2 c_{Li,anode}}{\partial x^2} \quad (2)$$

where $c_{Li,anode}$ is the lithium concentration and $D_{Li,anode}$ anode is the diffusion coefficient for lithium in the anode.

2.1.2 Cathode Modeling (NMC)

Porous Electrode Theory: The cathode is modeled using a macro-homogeneous porous electrode model with the following equation for lithium-ion transport:

$$\frac{\partial c_{Li,cathode}}{\partial t} = \nabla\cdot\left(D_{Li,cathode}\,\nabla c_{Li,cathode}\right) - \frac{1}{F}\nabla\cdot j_{Li,cathode} \quad (3)$$

where $c_{Li,cathode}$ is the lithium-ion concentration in the cathode, $D_{Li,cathode}$ is the effective diffusion coefficient, and $j_{Li,cathode}$ cathode is the lithium-ion flux.

Charge Transfer Kinetics: The Butler-Volmer equation for the cathode is similarly defined, with parameters specific to the cathode materials and reactions.

2.1.3 Polymer Electrolyte Modeling

Effective Medium Theory: The theory describes a sophisticated method to calculate the ionic conductivity of the hybrid electrolyte system [9, 10]. We followed the method adopted in the paper [11] where Effective Medium Theory (EMT) was applied to a hybrid solid electrolyte system, incorporating a polymer matrix with dispersed ceramic particles. The theory defines the overall ionic conductivity of the hybrid electrolyte using a model that accounts for the conductivity contributions of the polymer (σ_p), the ceramic particles (σ_{np}), and an interfacial layer (σ_i).

From the paper [11], the overall ionic conductivity for the hybrid electrolyte can be calculated using the following equations:

$$\sigma = \frac{\sqrt{\sigma_p n - A + \sqrt{A^2 + 2\tau(z^{-2} - zV_{np})}}}{z^{-2}} \quad (4)$$

where A and τ are defined as:

$$A = \frac{1 - zV_p + \tau(1 - zV_i)}{2} \quad (5)$$

$$\tau = \frac{\sigma_i}{\sigma_p} \quad (6)$$

Here, *z* is the coordination number, and V_{np} and V_p, and V_i are the volumetric fractions of the inorganic particles, polymer, and interphase region, respectively.
The volume of the inorganic particles (V_{np}) in the hybrid electrolyte is given by:

$$V_{np} = p \quad (7)$$

where *p* is the volume fraction of the inorganic particles.
The volumetric distribution of the polymer (V_p) and interphase region (V_i) can be calculated by:

$$V_p = (1-p)\eta^d \quad (8)$$
$$V_i = 1 - p - (1-p)\eta^d \quad (9)$$

where η is the ratio of the particle radius plus the interfacial layer thickness to the particle radius, $\eta = \frac{R+\lambda}{R}$ and *d* represents the model dimensions, which is 3 for a three-dimensional case.
These equations consider the complex interactions between the polymer matrix, the ceramic particles, and the interfacial layer. They provide a comprehensive way to predict the effective ionic conductivity of the hybrid electrolyte, which is crucial for the performance of batteries with solid polymer electrolytes.

Electrolyte-Electrode Interface
Interfacial Current Density: At the solid-solid interface between the polymer electrolyte and the electrodes, the interfacial current density $i_{interface}$ is described by a modified Butler-Volmer equation for solid-state interfaces:

$$i_{interface} = i_{o,interface}\left[\exp\left(\frac{\alpha_a F}{RT}\Delta\phi_{s-s}\right) - \exp\left(\frac{\alpha_c F}{RT}\Delta\phi_{s-s}\right)\right] \quad (10)$$

Here, $i_{interface}$ is the interfacial current density, $i_{o,interface}$ is the exchange current density at the solid-solid interface, α_a and α_c are the charge transfer coefficients, *F* is Faraday's constant, *R* is the universal gas constant, *T* is the temperature, and $\Delta\phi_{s-s}$ is the potential difference across the solid-solid interface.

2.1.4 Numerical Solution and Boundary Conditions

The boundary conditions used in the electrochemical model are listed below:
The boundary condition “ground”, corresponding to Equation (11), is applied to define a reference potential within the model. In the analysed case, this boundary condition is directly applied at the negative electrode of the cell, the Li metal, in order to define the cell voltage according to Equation 12.

$$\phi_s = 0 \quad (11)$$
$$E_{cell} = \phi_{s,cathode} - \phi_{s,anode} \quad (12)$$

The boundary condition “charge-discharge cycle” is applied at the extreme of the positive current collector to model the galvanostatic cycling behavior of the cell. A positive current and the maximum voltage (4.2 V) were employed for the charge, while a negative current and the minimum voltage (3.0 V) were applied for the discharge.

The modeling frameworks discussed earlier are prevalent for conventional lithium-ion batteries (LIBs). However, certain inherent constraints become more pronounced when these models are applied to solid-state lithium metal batteries. These constraints include:

- **Anode Reaction Dynamics**: The kinetic processes at the anode are intricate, particularly due to the lithium plating and stripping mechanisms, which the model does not fully capture.
- **Interfacial Consistency and Mechanical Response**: The interface contact between different layers and the mechanical properties of the composite electrolyte present challenges, especially considering the solid-solid interactions that are not accounted for in this model.
- **Transport Mechanisms in Composite Electrolytes**: The ion transport within the composite solid electrolyte is more complex due to the heterogeneous nature of the materials, requiring a model that can address the varying conductivities and interface phenomena.

2.1.5 Calibration and Validation

Based on the experimental data of cell size and dimension obtained from WP6, the electrochemical electrolyte data for L2 HCPE Gen1 cells were obtained from WP5, and the electrode data came from WP4. The data obtained from different work packages were added to the model. The data of charge and discharge curves is used to validate the model. The cells were charged and discharged at C/20 at 60 °C.

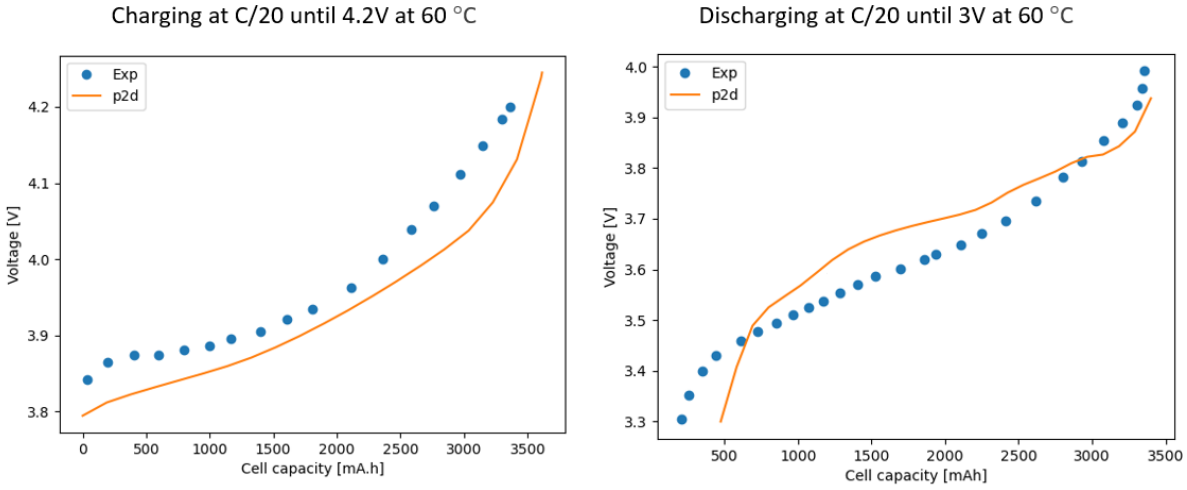

Figure 2 Charge discharge curves at C/20 for 3.35Ah pouch cell and their comparison with the P2D model.

In Figure 2, the charging graph reveals a notable divergence of the P2D model from the experimental data as the cell approaches full capacity, which can be attributed to the P2D model's omission of mechanical forces. Such forces can induce stress and strain within the cell, affecting electrode-electrolyte contact and contributing to increased internal resistance, which is not accounted for in the model. This discrepancy is also evident in the discharging graph, where the P2D model initially mirrors the experimental trend but deviates, particularly in the mid-capacity range, before reconverging near the end of discharge.
This deviation may also stem from other factors not incorporated into the model, including the formation and evolution of the solid electrolyte interphase (SEI) layer, alterations in electrode microstructure during cycling, non-uniform temperature distribution, and variations in ionic transport efficiency due to inhomogeneities within the solid electrolyte. Additionally, electrolyte decomposition and side reactions, more pronounced at extreme voltages or states of charge, could further contribute to the observed disparities.

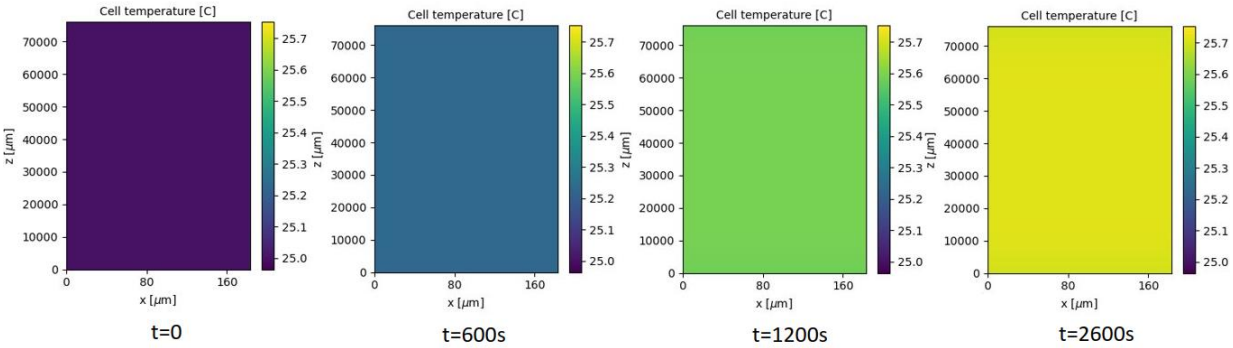

Figure 3 Temperature evolution with time within the cell for discharge at C/5 until 3.0 V.

Figure 2 above displays temperature profiles of a battery cell at different times during a discharge cycle at a C/5 rate. Each panel represents a time snapshot, starting from t = 0 and ending at t = 2600 seconds. The color coding indicates the cell's temperature:
At t = 0, the cell begins at a uniform temperature.
At t = 600 s, the temperature starts to increase, suggesting the onset of the discharge process.
By t = 1200 s, the temperature has increased further, as shown by the color change.
At t = 2600 s, the color indicates the highest temperature, suggesting significant heat generation during discharge.
Uniform color across the cell suggests even temperature distribution, a positive indicator of thermal management within the cell. Thermal tests were performed by IKERLAN and are reported in D9.5. Their results suggest that charging and discharging at lower C-rate does not result in a huge temperature change within the cell. Our model confirms this result.

3 Results and Discussion

Sensitivity Analysis

Earlier in this project, the P2D model was developed by CID at the coin cell level for L1 materials. In this work, we developed a P2D model for a 3.35 Ah pouch cell developed by SAFT in SAFELiMOVE project. To understand the issues of upscaling from coin cells to larger pouch cells, a sensitivity analysis of key changeable parameters such as electrolyte diffusivity, positive electrode thickness, positive electrode porosity, and electrolyte conductivity has been done to address the issues in upscaling.

Symbol	Design variable	Distribution	Range	Units
ε_c	Cathode porosity	uniform	$[0.2, 0.8]$	-
L_c	Cathode thickness	uniform	$[60, 180]$	μm
D_e	Electrolyte diffusivity	log-uniform	$[9.36 \cdot 10^{-13}, 2.26 \cdot 10^{-11}]$	$m^2/_s$
κ	Electrolyte ionic conductivity	log-uniform	$[1.32 \cdot 10^{-5}, 5.93 \cdot 10^{-2}]$	$S/_m$

Table 1 Different design parameters with their range to analyze their sensitivity.

Electrolyte diffusivity

Figure 4 presents a series of discharge curves for a battery at a C/5 rate until the terminal voltage reaches 3V, with each curve corresponding to a different electrolyte diffusivity.

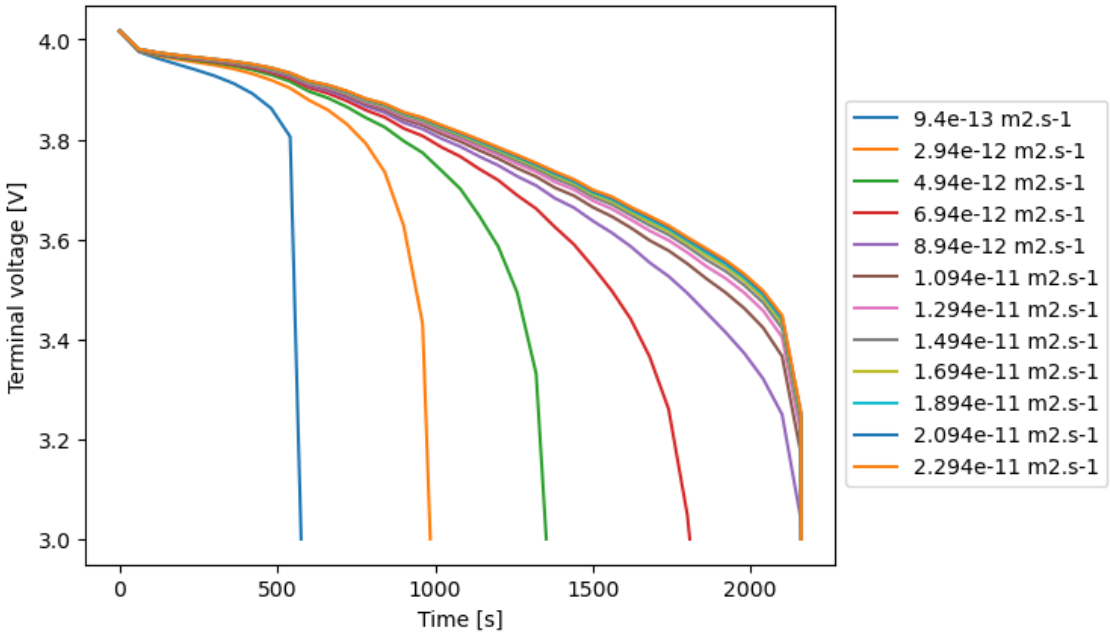

Figure 4 Discharge curve at C/5 until 3V for different electrolyte diffusivity.

All curves exhibit an initial rapid drop in voltage, which is common as the internal resistance of the battery causes an immediate fall in voltage upon discharge. As the diffusivity increases, the curves become steeper during discharge. Higher diffusivity likely results in faster ion transport, which could lead to quicker depletion of the available lithium ions near the electrodes [12], hence the steeper voltage drop. After the initial drop, the curves tend to flatten out, forming a plateau. This is characteristic of battery chemistry and indicates a period of relatively stable discharge. However, the length and slope of the plateau vary with diffusivity, where lower diffusivity appears to shorten the plateau phase.

Towards the end of discharge, all curves trend downwards more steeply as they approach the cut-off voltage of 3.0 V. This is typical as the cell exhausts its charge, but the rate of decline varies, with higher diffusivity curves reaching the cut-off voltage quicker.

There is a clear separation between the curves based on the diffusivity values, especially noticeable in the mid to later stages of discharge. This separation could be indicative of how diffusivity affects the rate of ion transport throughout the entire discharge process[13]. The results suggest that high electrolyte diffusivity is important to achieve sufficient ion transport within the cell.

Electrolyte ionic conductivity

Figure 5 Discharge curve at C/5 until 3V for different electrolyte ionic conductivity. illustrates discharge curve at C/5 until 3.0 V for different electrolyte ionic conductivity illustrates battery discharge curves at a C/5 rate down to 3.0 V under a constant temperature of 60 °C, with each curve representing a different ionic conductivity of the electrolyte.

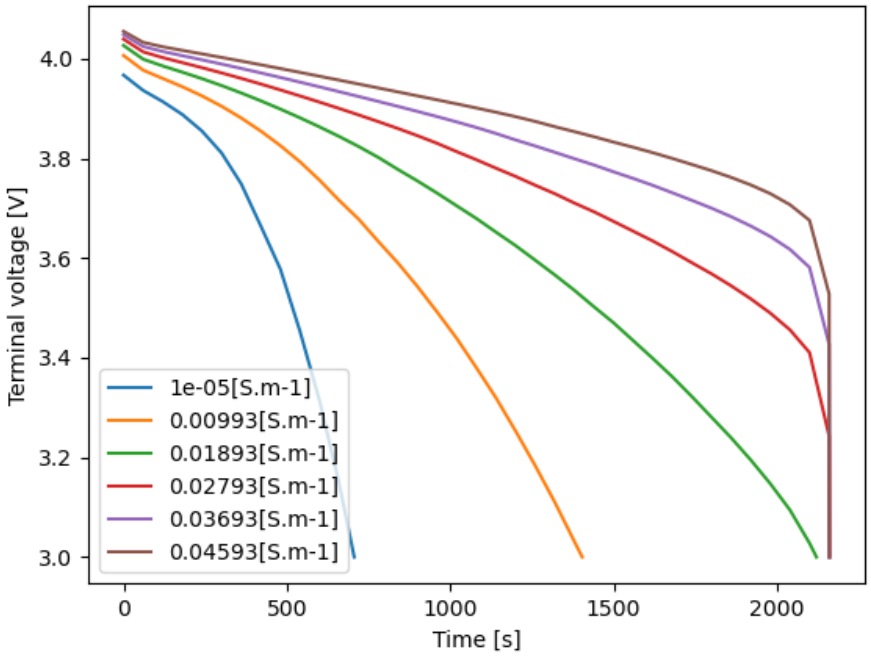

Figure 5 Discharge curve at C/5 until 3V for different electrolyte ionic conductivity.

Curves begin with a similar voltage, indicating a consistent open-circuit voltage across the different electrolyte conductivities. The voltage drop becomes steeper with increasing ionic conductivity. This suggests that higher ionic conductivity allows for more rapid ion transport, leading to faster utilization of the electrochemical potential within the cell. As with the previous graph, there's a mid-discharge voltage plateau. However, in Figure 4, lower ionic conductivities lead to a more pronounced and earlier departure from the plateau, indicating a more rapid transition from the nominal voltage to end-of-discharge voltage levels. The curves show that cells with lower ionic conductivities reach the cut-off voltage faster [14], confirming the trend observed in the previous graph. There is a convergence of the curves as they approach the cut-off voltage. This could indicate that at lower voltages, the battery's internal resistance or kinetics of the electrochemical reactions become the limiting factors, overshadowing the effects of electrolyte conductivity. By comparing both graphs, it becomes evident that increased diffusivity and conductivity can enhance the rate of ion transport and potentially improve power delivery.

Positive electrode thickness

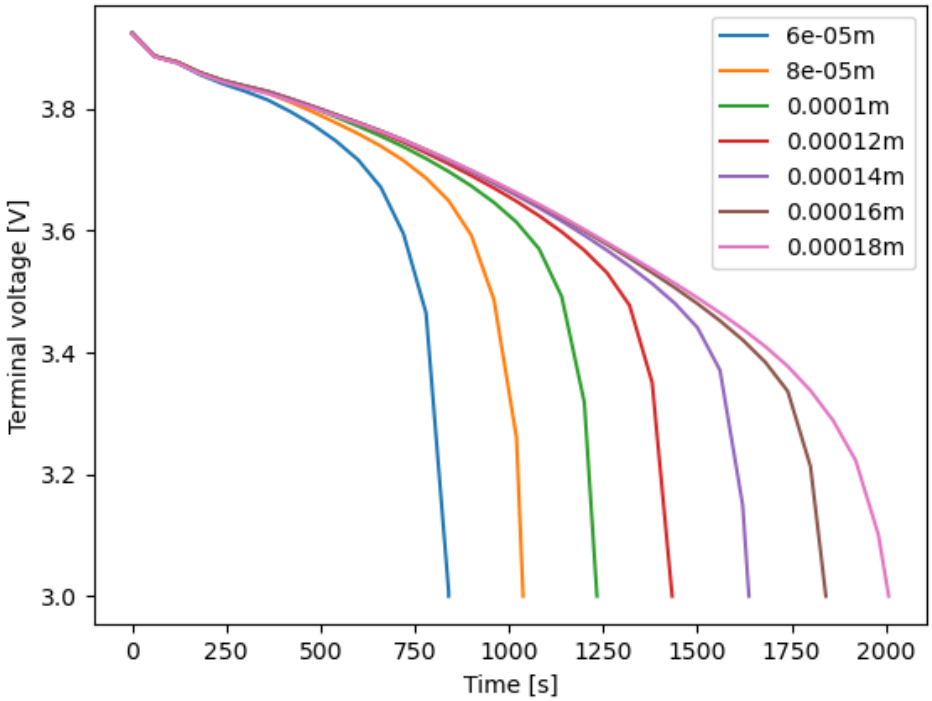

Figure 6 Discharge curve at C/5 until 3V for different positive electrode thicknesses.

In Figure 6, curves reveal that thicker electrodes lead to a slower discharge profile. This is evident as the curves associated with higher thicknesses (e.g., 0.00018 m, i.e. 180 µm) remain higher for a longer period compared to those with thinner electrodes. All curves exhibit a typical voltage decline during discharge. However, the rate of voltage drop varies with electrode thickness, with thinner electrodes experiencing a more rapid decline.

As the discharge progresses, especially past the mid-point, the curves begin to converge. This suggests that while electrode thickness influences the initial discharge behavior, other factors such as electrolyte depletion or internal resistance become dominant as the cell approaches complete discharge.

Thicker electrodes generally correspond to a higher energy capacity, as they can hold more active material. However, the curves indicate a trade-off, as thicker electrodes also seem to discharge more slowly, possibly due to limitations in ion diffusion through the thicker electrode material [15].

Correlating with the earlier graphs on electrolyte diffusivity and conductivity, this graph (Figure 5) supports the notion that internal cell components and materials significantly influence discharge characteristics. While higher diffusivity and conductivity facilitate faster ion transport, the increased thickness in electrodes seems to counteract this effect by prolonging the discharge, likely due to slower diffusion in the solid phase.

Porosity of positive electrode

In Figure 7, higher porosity levels appear to result in a slower discharge rate, as indicated by the curves that remain higher for longer durations. This could be due to increased electrolyte volume, which can sustain ion transport for longer periods. Like in the previous graphs, a voltage plateau is observed, where the rate of voltage decline is relatively steady. The plateau's duration and slope vary with porosity, which can be linked to the porosity's effect on ion diffusion and electrode utilization.

As the curves approach the terminal voltage, they steepen and converge, suggesting that regardless of porosity, all cells eventually reach a similar depletion rate as they near full discharge.

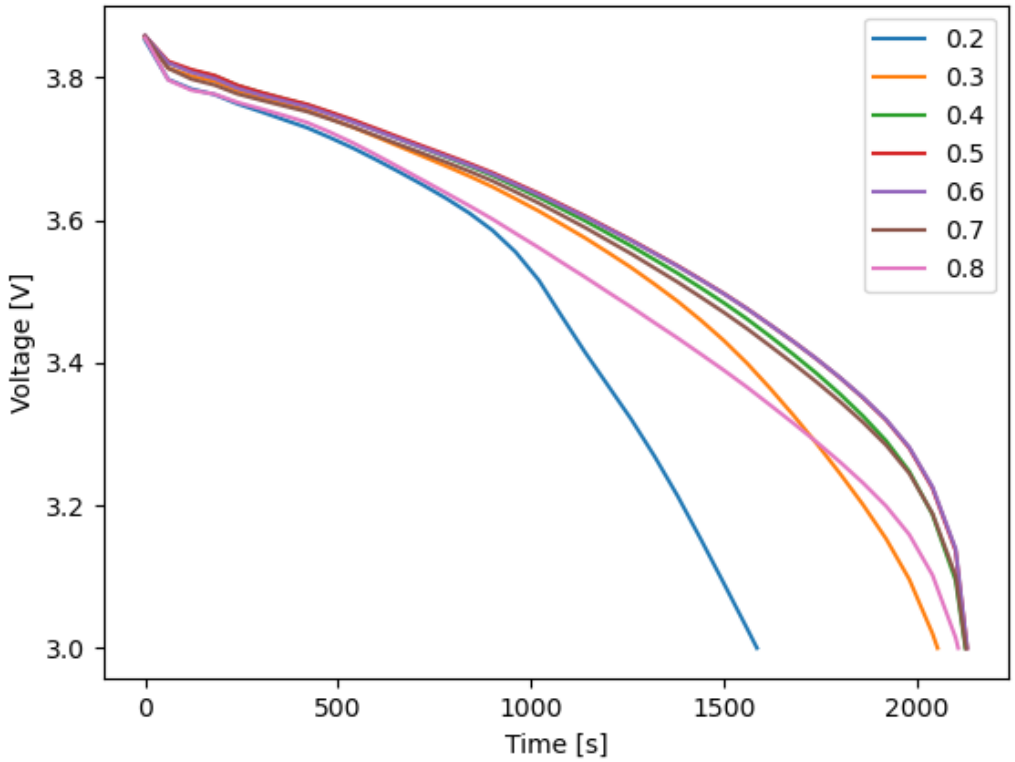

Figure 7 Discharge curve at C/5 until 3V for different porosities of positive electrode.

In comparing the various graphs depicting discharge curves based on different parameters—electrolyte diffusivity, ionic conductivity, electrode thickness, and porosity—the sensitivity of the battery's discharge profile to these parameters becomes evident. While electrolyte conductivity is a significant sensitivity factor in coin cells, pouch cells show a complex relationship between electrode porosity and discharge rates, suggesting that both electrolyte conductivity and electrode porosity are influential.

According to D9.1, for coin cells, higher electrolyte conductivity typically led to faster discharge rates, indicating that ion transport was the limiting factor. However, in pouch cells, electrode porosity plays an equally critical role, as it not only affects ion transport but also the mechanical stability and effective surface area for the electrochemical reactions.

This sensitivity analysis provides crucial insights into the upscaling from coin to pouch cells. The parameters that were most sensitive in coin cells may not hold the same level of influence in pouch cells due to differences in cell architecture, scale, and the increased importance of mechanical integrity and uniformity in larger cells.

As for dendrites, while the above results do not directly measure dendritic growth, the parameters influencing ion transport and electrode structure are closely related to dendrite formation. For instance, high ionic conductivity and appropriate porosity levels (High porosity in the cathode can improve ion transport, leading to more uniform lithiation and delithiation processes. This can help mitigate conditions that favor lithium plating at the anode, such as uneven ion distribution. Conversely, low porosity might lead to uneven ion flow and increased potential for lithium plating, especially under high charge rates or low temperatures.

The most sensitive parameter seems to vary with the scale and type of the cell. For coin cells, electrolyte conductivity was paramount, but as we move to pouch cells, the interplay between electrode porosity and electrolyte conductivity becomes more complex and equally critical. Optimizing these parameters in tandem could yield the best performance and longevity for pouch cells, with a focus on homogeneity to prevent local degradation such as dendrite formation. These insights are vital for the material suppliers and cell manufacturers to refine design and production processes as they upscale from coin to pouch cells.
The above results highlight several key performance aspects of battery cells, particularly the impact of material properties such as electrolyte diffusivity, conductivity, and electrode porosity. While the results do not directly measure interface quality or the effects of external pressure, we can infer their potential impact based on the behavior observed in the discharge curves.

Poor electrode-electrolyte interfaces can impede ion transport, which would be reflected in discharge curves as a faster voltage drop, similar to what is observed with low ionic conductivity.

A poor interface increases the cell's internal resistance, which could explain why some curves with higher porosity (which typically reduces resistance) still show quicker voltage decline — possibly due to poor contact points.

Variability in the discharge curves could be indicative of inhomogeneous interfaces across the cell. This would result in uneven ion flow and could also contribute to dendrite growth if certain areas permit higher ion concentrations.

The impact of External Pressure is well discussed in D9.5.

In summary, the analysis of discharge curves across a range of material properties underscores the importance of managing both the quality of interfaces and the application of external pressure. Poor interfaces can lead to increased resistance and inhomogeneous reaction rates, while external pressure must be carefully controlled to enhance interface contact without compromising electrode structure. These factors become even more critical when upscaling from coin to pouch cells, where the larger surface areas increase the probability of interface inconsistencies and the need for external pressure to maintain structural integrity. The sensitivity analysis thus provides indirect evidence that both interface quality and external pressure are pivotal in ensuring the uniformity and performance of larger-scale battery cells.

4 Conclusions and Recommendations

In conclusion, the upscaling of battery technology from coin cells to larger pouch cells necessitates a nuanced understanding of the interplay between various material properties and design parameters. Our exploration into the P2D model's extension to accommodate these larger formats has highlighted several critical factors. The sensitivity analysis conducted across different physical properties—electrolyte diffusivity, ionic conductivity, electrode thickness, and porosity—has revealed that while some factors like electrolyte conductivity maintain their prominence, others, such as electrode porosity, emerge with increased significance in the context of pouch cells.

The discharge curves generated under various conditions have served as a proxy to understand how these parameters influence overall cell performance. We observed that higher electrolyte diffusivity and conductivity tend to enhance discharge rates but may also reduce discharge duration, pointing to a trade-off between power and energy density. Similarly, electrode porosity must be carefully optimized to ensure mechanical stability and efficient ion transport, which are vital for maintaining performance over the cell's lifetime.

Furthermore, our discussions infer the potential impacts of poor interfaces and suboptimal external pressure on cell performance. Poor interfaces can significantly impede ion transport and increase internal

resistance, while external pressure must be judiciously applied to ensure good electrode-electrolyte contact and maintain electrode structure.

The insights gathered from our analysis are invaluable for material suppliers and cell manufacturers as they transition to producing larger cells. They underscore the need to consider a wider array of parameters and their compound effects on cell behavior. Notably, the balance between electrolyte conductivity and electrode porosity is critical in mitigating localized degradation phenomena such as dendrite formation.

Overall, the transition from coin to pouch cells is not merely a matter of scaling up but requires a reevaluation of design strategies and a more comprehensive modeling approach. The fine-tuning of these parameters will be crucial for the advancement of battery technology, ensuring that performance enhancements are realized without compromising safety or longevity. This work lays the groundwork for more robust and reliable battery cells capable of meeting the increasing demands of modern energy storage applications.

5 References

[1] N. Nitta, F. Wu, T. L. Lee and G. Yushin, "Li-ion battery materials: present and future," *Materials today,* vol. 18, no. 5, pp. 252-264, 2015.

[2] H. C. T. L. Y. K. A. B. J. C. a. Yeonguk Son, "Analysis of Differences in Electrochemical Performance Between Coin and Pouch Cells for Lithium-Ion Battery Applications," *Energy and Environment materials ,* pp. 12615-12620, 2023.

[3] T. F. F. a. J. N. M. Doyle, "Modeling of Galvanostatic Charge and Discharge of the Lithium/Polymer/Insertion Cell," *The Electrochemical Society,* pp. 1526-1532, 1993.

[4] S. M. V. S. C. P. a. S. C. R Timms, "Asymptotic Reduction of a Lithium-ion Pouch Cell Model," *Applied Physics,* 2020.

[5] J. N. a. K. Thomas-Alyea, Electrochemical Systems, John Wiley & Sons, 2012.

[6] J. N. a. C. Tobias, "Theoretical analysis of current distribution in porous electrodes," *Journal of The Electrochemical Society,* pp. 1183-1191, 1962.

[7] W. G. a. C. Wang, "Thermal-electrochemical modeling of battery systems," *Journal of The Electrochemical Society,* pp. 2910-2922, 2000.

[8] E. P. a. J. N. D. Bernardi, "A general energy balance for battery systems.," *Journal of The Electrochemical Society,* pp. 5-12, 1985.

[9] F. B. N. Z. 2. H. K. W. C. U. K. Somayeh Toghyani, "Model-Based Design of High Energy All-Solid-State Li Batteries with Hybrid Electrolytes," *Journal of The Electrochemical Society,* p. 040550, 2022.

[10] K. M. M. L. D. Stephanie Golmon, "Numerical modeling of electrochemical–mechanical interactions in lithium," *Computers and Structures,* p. 1567–1579, 2009.

[11] N. H. M. B. D. V. D. A. a. K. B. H. Wahid Zaman, "Visualizing percolation and ion transport in hybrid solid electrolytes for Li–metal batteries," *Journals of Materials Chemistry A,* pp. 23914-23921, 2019.

[12] E. K. Michael.J. Lain, "Understanding the limitations of lithium ion batteries at high rates," *Journal of Power Sources,* pp. 229690-229699, 2021.

[13] W. X. a. S. Yang, "Charging Optimization of Lithium-Ion Batteries Based on Charge Transfer Limitation and Mass Transport Limitation," *Journal of The Electrochemical Society,* pp. 010506-010511, 2023.

[14] D. D. D. J. H. T. P. G. B. P. M. W. a. P. E. P. a. Jaschar Atik, "Cation-Assisted Lithium-Ion Transport for High-Performance PEO-based Ternary Solid Polymer Electrolytes," *Angew Chem Int Ed Engl,* p. 11919–11927, 2021.

[15] H. C. J. S. a. Q. W. Wenxin Mei, "The effect of electrode design parameters on battery performance and optimization of electrode thickness based on the electrochemical–thermal coupling model," *Sustainiable energy and fuels,* pp. 148-165, 2019.

[16] M. W. A. V. L. Y. S. Y. Q. Daniel J. Noelle, "Internal resistance and polarization dynamics of lithium-ion batteries upon internal shorting," *Applied Energy,* pp. 796-808, 2018.

Appendix A- Acknowledgement

The author(s) would like to thank the partners in the project for their valuable comments on previous drafts and for performing the review.

Project partners:

#	Partner	Partner Full Name
1	CICe	CENTRO DE INVESTIGACION COOPERATIVA DE ENERGIAS ALTERNATIVAS FUNDACION, CIC ENERGIGUNE FUNDAZIOA
2	SCHOTT	SCHOTT AG
3	UMICORE	UMICORE
4	HYDRO-QUEBEC	HYDRO-QUEBEC
5	SAFT	SAFT
6	RENAULT SAS	RENAULT SAS
7	TME	TOYOTA MOTOR EUROPE NV
8	IKERLAN	IKERLAN S. COOP
9	CEA	COMMISSARIAT A L ENERGIE ATOMIQUE ET AUX ENERGIES ALTERNATIVES
10	CIDETEC	FUNDACION CIDETEC
11	TUB	TECHNISCHE UNIVERSITAT BERLIN
12	RWTH AACHEN	RHEINISCH-WESTFAELISCHE TECHNISCHE HOCHSCHULE AACHEN
13	ABEE	AVESTA BATTERY & ENERGY ENGINEERING
14	LCE Srl	LIFE CYCLE ENGINEERING SRL
15	UNIRESEARCH BV	UNIRESEARCH BV

Appendix B- Parameterization of L2 materials

Cathode properties	Value	Units
Thickness	20e-6	m
Electrolyte volume fraction	0.4	-
Bruggeman exponent	1.5	-
Active material volume fraction	0.5663	-
Electrical conductivity	0.337	S/m
Reaction rate coefficient	9e-12	$m^{3.5}/mol^{0.5}$ s
Active particle radius	2e-6	m
AM maximum Li concentration	24986	mol/m^3
AM initial Li concentration (100%SoC)	249.86	mol/m^3
AM Li Diffusivity	1e-16	m^2/s
AM Open circuit potential	Figure	V
AM Li Partial molar volume	1.2e-6	m^3/mol
AM Young modulus	375	GPa
AM Poisson ratio	0.2	-

Electrolyte properties	Value	Units
Initial salt concentration	1300	mol/m^3
Lithium-ion transference number	0.18	-
Electrolyte ionic conductivity	0.00014	S/m
Lithium-ion diffusion coefficient	3.3e-12	m^2/s
Partial molar volume	1.3e-4	m^3/mol

Lithium metal anode properties	Value	Units
Electro-deposition/dissolution reaction rate coefficient	5e-7	$m^{0.5}mol^{0.5}/s$
Conductivity	1e7	S/m
Molar volume	13e-6	m^3/mol
Young modulus	4.9	GPa
Poisson ratio	0.35	-